

Reactivity of $[\{\text{Mn}^{\text{IV}}(\text{salpn})\}_2(\mu\text{-O},\mu\text{-OCH}_3)]^+$ and $[\{\text{Mn}^{\text{IV}}(\text{salpn})\}_2(\mu\text{-O},\mu\text{-OH})]^+$: Effects of Proton Lability and Hydrogen Bonding

Michael J. Baldwin,[†] Neil A. Law, Timothy L. Stemmler, Jeff W. Kampf, James E. Penner-Hahn, and Vincent L. Pecoraro*

Department of Chemistry, The University of Michigan, Ann Arbor, Michigan 48109-1055

Received March 30, 1999

It was previously shown that the addition of 1 equiv of a strong acid to $[\text{Mn}^{\text{IV}}(\text{salpn})(\mu\text{-O})]_2$, **1**, generates the oxo/hydroxo complex $[\{\text{Mn}^{\text{IV}}(\text{salpn})\}_2(\mu\text{-O},\mu\text{-OH})](\text{CF}_3\text{SO}_3)$, **2**, which emphasized the basicity of the $\mu_2\text{-O}^{2-}$ units in the $[\text{Mn}^{\text{IV}}(\mu\text{-O})]_2$ dimers. We now demonstrate the inherent nucleophilicity of those $\mu_2\text{-O}^{2-}$ units by showing that the addition of methyl triflate to **1** results in formation of the oxo/methoxo-bridged Mn^{IV} dimer $[\{\text{Mn}^{\text{IV}}(\text{salpn})\}_2(\mu\text{-O},\mu\text{-OCH}_3)](\text{CF}_3\text{SO}_3)$, **3**. EXAFS analysis of **3** demonstrates that alkylation of an oxo bridge results in the same structural modification of the $[\text{Mn}^{\text{IV}}(\mu\text{-O})]_2$ core as an oxo bridge protonation. Electrochemical and spectroscopic comparisons of **3** to **2** indicate that **3** is a good electronic structure analogue for **2** without the complication of proton lability and hydrogen bonding. Indeed, **2** and **3** react nearly identically with hydrogen peroxide and with strong acids. In contrast, the products of their reactions with amines, acetate, and triphenylphosphine are dramatically different. The proton lability of **2** results in simple proton transfer, circumventing the slower redox reactions of these substrates with **3**. Isotopic labeling, kinetic, and EPR-monitored radical trap studies lead to a proposed reduction–oxidation mechanistic scheme for the reactions of **3** with amines and triphenylphosphine. The Mn^{III} product of this reaction, $[\text{Mn}^{\text{III}}(\text{salpn})(\text{Ph}_3\text{PO})](\text{CF}_3\text{SO}_3)$, was isolated and crystallographically characterized as a dimerized complex. The redox nature of the reactions is confirmed by trapping of a reduced Mn intermediate which is identified by EPR spectroscopy. Comparison of the reactions of **2** and **3** demonstrates the dramatic effect of proton lability and hydrogen bonding on reactivity, and suggests how metalloenzymes may regulate active site reactivity to produce very different catalytic activities with similar active site structures. Furthermore, it also emphasizes that caution should be used when the reactivity of model compounds with easily and rapidly dissociable protons is assessed.

Introduction

The oxygen-evolving complex (OEC) is a tetranuclear manganese cluster that catalyzes the transfer of four reducing equivalents from two water molecules to the photosynthetic apparatus in green plants, with evolution of molecular oxygen and the release of four protons.^{1–10} This oxidation of water to molecular oxygen is a very high potential reaction (3.6 V total

energy transfer, $\text{pH} \approx 6$).¹¹ Movement of protons during this reaction cycle is believed to be critical to accommodating storage of the oxidation equivalents until the entire 3.6 V is accumulated through four one-electron transfers. The tetranuclear Mn cluster in the OEC is thought to be comprised of a pair of bis(oxo)-bridged Mn dimers in high oxidation states (Mn^{III} and Mn^{IV}).^{12–14} The Mn ions within those dimeric units are separated by 2.7 Å.^{12–14} The “dimer of dimers” model suggests that those $[\text{Mn}_2\text{O}_2]$ dimers are then linked via a combination of oxo and carboxylato bridges on the basis of the 3.3 Å Mn–Mn distance reported from EXAFS data on PSII samples.^{12–14} To understand the role of protons in the OEC better, we have employed the bis(oxo)-bridged Mn^{IV} dimer $[\text{Mn}^{\text{IV}}(\text{salpn})(\mu\text{-O})]_2$, **1**, as a model for the OEC.^{15–21} This model compound has the same 2.7 Å

* To whom correspondence should be addressed.

[†] Current address: Department of Chemistry, University of Cincinnati, Cincinnati, OH 45221-0172.

- (1) Yocum, C. F.; Pecoraro, V. L. *Curr. Opin. Chem. Biol.* **1999**, *3*, 182–187.
- (2) *Oxygenic Photosynthesis: The Light Reactions*; Ort, D. R., Yocum, C. F., Eds.; Kluwer Academic Publishers: Boston, 1996.
- (3) Britt, R. D. In *Oxygenic Photosynthesis: The Light Reactions*; Ort, D. R., Yocum, C. F., Eds.; Kluwer Academic Publishers: Boston, 1996; pp 137–164.
- (4) Yachandra, V. K.; Sauer, K.; Klein, M. P. *Chem. Rev.* **1996**, *96*, 2927–2950.
- (5) Debus, R. J. *Biochim. Biophys. Acta* **1992**, *1102*, 269–352.
- (6) *Manganese Redox Enzymes*; Pecoraro, V. L., Ed.; VCH Publishers, Inc.: New York, 1992.
- (7) Law, N. A.; Caudle, M. T.; Pecoraro, V. L. In *Advances in Inorganic Chemistry*; Sykes, A. G., Ed.; Academic Press: New York, 1999; Vol. 46, pp 305–440.
- (8) Pecoraro, V. L.; Baldwin, M. J.; Gelasco, A. *Chem. Rev.* **1994**, *94*, 807–826.
- (9) Pecoraro, V. L.; Hsieh, W.-Y. In *Manganese and Its Role in Biological Processes*; Sigel, A., Sigel, H., Ed.; Marcel Dekker: New York, Vol. 37, in press.
- (10) Wieghardt, K. *Angew. Chem., Int. Ed. Engl.* **1989**, *28*, 1153–1172.

- (11) Babcock, G. T.; Barry, B. A.; Debus, R. J.; Hoganson, C. W.; Atamian, M.; McIntosh, L.; Sithole, I.; Yocum, C. F. *Biochemistry* **1989**, *28*, 9557–9565.
- (12) Penner-Hahn, J. E. In *Structure and Bonding*; Hill, H. A. O., Sadler, P. J., Thomson, A. J., Eds.; Springer Verlag: Berlin, 1998; Vol. 90, pp 1–36.
- (13) Penner-Hahn, J. E.; Fronko, R. M.; Pecoraro, V. L.; Yocum, C. F.; Betts, S. D.; Bowlby, N. R. *J. Am. Chem. Soc.* **1990**, *112*, 2549–2557.
- (14) Klein, M. P.; Sauer, K.; Yachandra, V. K. *Photosynth. Res.* **1993**, *38*, 265–278.
- (15) Larson, E. J.; Pecoraro, V. L. *J. Am. Chem. Soc.* **1991**, *113*, 3810–3818.
- (16) Larson, E. J.; Riggs, P. J.; Penner-Hahn, J. E.; Pecoraro, V. L. *J. Chem. Soc., Chem. Commun.* **1992**, 102–103.
- (17) Larson, E.; Lah, M. S.; Li, X.; Bonadies, J. A.; Pecoraro, V. L. *Inorg. Chem.* **1992**, *31*, 373–378.

separation as the OEC,¹⁷ and is an effective catalyst of hydrogen peroxide disproportionation.^{15,22} This reaction has been proposed as a model for the catalase activity attributed to the OEC,²³ although recent research suggests that this catalase chemistry may in fact be due to a membrane-associated heme catalase.^{24,25}

We have shown previously that **1** may be protonated¹⁶ once to form $[\{\text{Mn}^{\text{IV}}(\text{salpn})\}_2(\mu\text{-O}, \mu\text{-OH})(\text{CF}_3\text{SO}_3)_2]$, **2**, or twice to form $[\text{Mn}^{\text{IV}}(\text{salpn})(\mu\text{-OH})_2(\text{CF}_3\text{SO}_3)_2]$, **4**.¹⁹ We have used this series of complexes to show the effects of successive protonations on the spectroscopic, magnetic, and structural properties of $[\text{Mn}^{\text{IV}}(\mu\text{-O})_2]$ units similar to those in the OEC.^{16,19} We have shown the intimate relationship between the redox properties and acid–base properties of these systems.¹⁸ We also have determined $\text{p}K_a$ values and reduction potentials of these complexes to calculate homolytic O–H bond dissociation energies (BDEs), which demonstrated the feasibility of either a hydrogen atom transfer mechanism or a proton-coupled electron transfer for oxidation-state advancement in the OEC,^{20,21,26} as proposed independently by Babcock^{27–30} and Britt.^{31–34}

Our attempts to study the detailed effects of protonation on the reactivity of **1**, **2**, and **4** were hindered by the lability of the protons. Transfer of protons from unreacted substrates to more basic products prevents completion of the reactions and often results in a mixture of species that is difficult to characterize. To circumvent the complication of proton lability in studying these reactions, the methylated analogue of **2**, $[\{\text{Mn}^{\text{IV}}(\text{salpn})\}_2(\mu\text{-O}, \mu\text{-OCH}_3)](\text{CF}_3\text{SO}_3)_2$, **3**, was synthesized. In addition to the benefit of the lack of lability of the methyl group, substitution of the methyl group for the proton results in greater solubility in organic solvents.

In this paper we present the synthesis and characterization of **3**, and describe its use as a probe of the effects of protonation on the reactivity of $[\text{Mn}^{\text{IV}}(\mu\text{-O})_2]$. Comparison of the spectroscopic and electrochemical properties of **3** to those of **2** shows that their electronic structures are nearly identical. Indeed, their reactivities with some substrates, such as hydrogen peroxide, appear to be nearly identical as well. Other reactions of **2** and

3 are dramatically different, however, including reaction with amines, which have been shown to inactivate the OEC.³⁵

Experimental Section

Materials. All amines, tetramethylammonium acetate, triphenylphosphine, and triphenylphosphine oxide were used as provided by Aldrich. Acetonitrile was prepared for use by stirring over anhydrous CuSO_4 to remove trace amines, then predried over CaH_2 , and distilled from P_2O_5 . Methylene chloride was distilled from CaH_2 . $[(\text{CH}_3)_4\text{N}][\text{Zn}(\text{PhS})_4]$ was prepared by a slight modification of the preparation by Dance et al.³⁶ $[\text{Mn}^{\text{IV}}(\text{salpn})(\mu\text{-O})_2]$, **1**,¹⁵ and $[\{\text{Mn}^{\text{IV}}(\text{salpn})\}_2(\mu\text{-O}, \mu\text{-OH})(\text{CF}_3\text{SO}_3)_2]$, **2**,^{16,19} were prepared as described previously.

$[\{\text{Mn}^{\text{IV}}(\text{salpn})\}_2(\mu\text{-O}, \mu\text{-OCH}_3)](\text{CF}_3\text{SO}_3)_2$, **3**, was prepared by addition of a several-fold excess (10 drops from a Pasteur pipet) of 99+% methyl triflate (Aldrich, used as supplied and stored refrigerated under argon after opening) to a 0.7 mM solution of **1** (0.22 g) in 400 mL of distilled CH_2Cl_2 . The solution was stirred for 10–16 h. The dark purple-brown solution was filtered, and the solvent was concentrated to 10 mL by rotary evaporation at 30–35 °C. The concentrated solution was brought up in 100 mL of a 1:1 $\text{CHCl}_3/\text{Et}_2\text{O}$ mixture and stirred for 15 min. This solution was filtered, separating a deep purple solution from a brown solid that was discarded. The solution was concentrated under a stream of dry nitrogen to 10 mL. A 200 mL sample of diethyl ether was added, and the purple precipitate was collected by vacuum filtration and rinsed with diethyl ether. Yield: 98 mg, 35%. Elemental analysis: Obsd Mn, 12.1; C, 48.6; H, 4.3; N, 6.3. Calcd (for $3 \cdot \text{H}_2\text{O}$, MW 884.6) Mn, 12.4; C, 48.9; H, 4.2; N, 6.2. FAB⁺MS: strong peak at m/z 717 (parent cation of **3**), with no peak at m/z 703 (parent cation of **2**).

$[\text{Mn}^{\text{III}}(\text{salpn})(\text{Ph}_3\text{PO})](\text{CF}_3\text{SO}_3)_2$, **6**, was prepared by the addition of 58 mg (0.2 mmol) of Ph_3PO to a solution of 55 mg (0.1 mmol) of $[\text{Mn}^{\text{III}}(\text{salpn})(\text{H}_2\text{O})_2](\text{CF}_3\text{SO}_3)_2$, **7**, in 10 mL of distilled acetonitrile. This mixture was stirred at room temperature until all of the Ph_3PO had dissolved, and a green-brown solution had formed. Addition of diethyl ether precipitated a green solid. This was collected by vacuum filtration and washed with benzene to remove excess Ph_3PO . Yield: 51 mg, 85%. Elemental analysis: Obsd Mn, 7.6; C, 57.0; H, 4.2; N, 3.7. Calcd (MW 762.6) Mn, 7.2; C, 56.7; H, 4.1; N, 3.7. FAB⁺MS: strong peak at m/z 613. X-ray quality, brown, block-like crystals of **6** were grown from a solution of dichloromethane/benzene at room temperature.

$[\text{Mn}^{\text{III}}(\text{salpn})(\text{H}_2\text{O})_2](\text{CF}_3\text{SO}_3)_2$, **7**, was prepared by a modification of the synthesis reported for $[\text{Mn}^{\text{III}}(\text{salpn})(\text{CH}_3\text{OH})_2](\text{ClO}_4)_2$.¹⁵ In 25 mL of methanol was slurried 2.0 g (4.6 mmol) of $[\text{Mn}^{\text{III}}(\text{salpn})(\text{acac})_3]$.¹⁵ To this was added 0.71 g (4.6 mmol) of 98% trifluoromethanesulfonic acid that had been diluted in 10 mL of methanol. The resulting solution was stirred for 15 min, and the solution was reduced to a residue by rotary evaporation of the solvent. This was redissolved in 100 mL of an 80:20 mixture of $\text{CHCl}_3/\text{diethyl ether}$, and was decanted from an oily residue. To the chloroform/ether solution was added 5 mL of methanol, and the resulting solution was allowed to stand for several days to allow the microcrystalline product to precipitate (typical yields $\geq 50\%$). Elemental analysis: Obsd Mn, 10.1; C, 40.3; H, 4.0; N, 5.2. Calcd (for $7 \cdot \text{H}_2\text{O}$, MW 538.4) Mn, 10.2; C, 40.2; H, 4.1; N, 5.2.

Methods. UV/vis absorption spectra of stable solutions were collected on a Perkin-Elmer Lambda 9 spectrophotometer. Spectra of unstable solutions (such as **4** and $[\{\text{Mn}^{\text{IV}}(\text{salpn})\}_2(\mu\text{-OH}, \mu\text{-OCH}_3)](\text{CF}_3\text{SO}_3)_2$, **5**) were collected by mixing reactants with an OLIS stopped-flow apparatus and collecting spectra of the initial mixture within 10 ms, prior to decomposition, using an OLIS rapid-scanning monochromator. This same system was used for collecting rapid kinetic data for the reactions of **3** with various bases. Typical experiments mixed a 0.1 mM solution of **3** in CH_3CN with a 5 mM solution of base in CH_3CN . In experiments with added H_2O or D_2O , 0.1% (55 mM) water was added to the solution of **3** prior to introduction of the samples to the stopped-flow apparatus. Comparison of the relative overall reaction rates was accomplished by fitting the data to a simple single-exponential

- (18) Baldwin, M. J.; Gelasco, A.; Pecoraro, V. L. *Photosynth. Res.* **1993**, *38*, 303–308.
 (19) Baldwin, M. J.; Stemmler, T. L.; Riggs-Gelasco, P. J.; Kirk, M. L.; Penner-Hahn, J. E.; Pecoraro, V. L. *J. Am. Chem. Soc.* **1994**, *116*, 11349–11356.
 (20) Baldwin, M. J.; Pecoraro, V. L. *J. Am. Chem. Soc.* **1996**, *118*, 11325–11326.
 (21) Pecoraro, V. L.; Baldwin, M. J.; Caudle, M. T.; Hsieh, W.-Y.; Law, N. A. *Pure Appl. Chem.* **1998**, *70*, 925–929.
 (22) Larson, E. J.; Pecoraro, V. L. *J. Am. Chem. Soc.* **1991**, *113*, 7809–7810.
 (23) Frasch, W. D.; Mei, R. *Biochim. Biophys. Acta* **1987**, *891*, 8–14.
 (24) Sheptovitsky, Y. G.; Brudvig, G. W. *Biochemistry* **1996**, *35*, 16255–16263.
 (25) Sheptovitsky, Y. G.; Brudvig, G. W. *Biochemistry* **1998**, *37*, 5052–5059.
 (26) Caudle, M. T.; Pecoraro, V. L. *J. Am. Chem. Soc.* **1997**, *119*, 3415–3416.
 (27) Tommos, C.; Tang, X.-S.; Warncke, K.; Hoganson, C. W.; Styring, S.; McCracken, J.; Diner, B. A.; Babcock, G. T. *J. Am. Chem. Soc.* **1995**, *117*, 10325–10335.
 (28) Hoganson, C. W.; Lydakis-Simantiris, N.; Tang, X.-S.; Tommos, C.; Warncke, K.; Babcock, G. T.; Diner, B. A.; McCracken, J.; Styring, S. *Photosynth. Res.* **1995**, *46*, 177–184.
 (29) Hoganson, C. W.; Babcock, G. T. *Science* **1997**, *277*, 1953–1956.
 (30) Tommos, C.; Babcock, G. T. *Acc. Chem. Res.* **1998**, *31*, 18–25.
 (31) Gilchrist, M. L.; Ball, J. A.; Randall, D. W.; Britt, R. D. *Proc. Nat. Acad. Sci. U.S.A.* **1995**, *92*, 9545–9549.
 (32) Tang, X.-S.; Randall, D. W.; Force, D. A.; Diner, B. A.; Britt, R. D. *J. Am. Chem. Soc.* **1996**, *118*, 7638–7639.
 (33) Force, D. A.; Randall, D. W.; Britt, R. D. *Biochemistry* **1997**, *36*, 12062–12070.
 (34) Peloquin, J. M.; Campbell, K. A.; Britt, R. D. *J. Am. Chem. Soc.* **1998**, *120*, 6840–6841.

- (35) Beck, W. F.; Sears, J.; Brudvig, G. W.; Kulawiec, R. J.; Crabtree, R. H. *Tetrahedron* **1989**, *45*, 4903–4911.
 (36) Dance, I. G.; Chan, A.; Scudder, M. L. *J. Am. Chem. Soc.* **1984**, *106*, 6285–6295.

decay. The rate constants for the single exponential are reported for various reactions under the same concentration and solvent conditions. These rate constants are used simply to compare overall rates of the reactions, and the absolute values (which are uncorrected for concentration, absorption coefficient, and cell path length, which are the same in each experiment) are not intended to relate directly to a proposed reaction mechanism.

Reactions of **3** with Ph_3P were run as follows: 10 mg each of Ph_3P and **3** were combined as solids. 4 mL of CH_2Cl_2 was added, and the sample was mixed by gentle shaking and allowed to stand until the solution turned from purple to brown (about 10 min). This was done either in the air or under a nitrogen atmosphere using degassed solvent. The Ph_3PO product was identified by FAB^+ (fast atom bombardment) mass spectrometry. The yield of Ph_3PO was determined by comparing the gas chromatograph of the product solution to a titration curve of a series of $\text{Ph}_3\text{P}/\text{Ph}_3\text{PO}$ mixtures of varying ratios that maintained the same total phosphorous concentration as in the reaction with **3**. In experiments with isotopically labeled water in solution, the labeled or unlabeled water was added to the solvent to 40 mM prior to solvation of the solid reactants.

Cyclic voltammograms were collected on a BAS 100 electrochemical analyzer. Voltammograms of **1**, **2**, **3**, and **5** were determined for 1 mM solutions in CH_2Cl_2 (**1**, **3**, and **5**) or CH_3CN (**3** and **2**). Comparison of **3** and **5** was done at -35°C vs silver wire (-140 mV vs ferrocene under these conditions). CVs of **1**, **2**, and **3** were collected at room temperature vs SCE electrode. CVs of the bases and triphenylphosphine were collected on 10 mM samples in CH_3CN . All experiments were done using a Pt auxiliary electrode, a glassy carbon working electrode, and 100 mM $(\text{Bu}_4\text{N})(\text{PF}_6)$ as electrolyte (except the comparison between **3** and **5**, which used $(\text{Bu}_4\text{N})(\text{CF}_3\text{SO}_3)$). Scan rates were 100 mV/s.

The N(or O)–H bond dissociation energies of the protonated bases, listed in Table 3, were determined, on the basis of their measured reduction potentials and $\text{p}K_a$ values,³⁷ by the method reported in refs 20 and 26.

Incorporation or loss of ^{18}O isotopic labels was monitored by fast atom bombardment (FAB) mass spectrometry. Samples were dissolved in a small amount of an appropriate solvent and then introduced into a 3-nitrobenzyl alcohol matrix. FAB^+ detection was used for **3**, **2**, and Ph_3PO , and FAB^- detection was used for **1**. In each case, the relatively strong parent ion peak was used for the analysis. The mass spectra were collected on a VG Instruments VG 70-250-S mass spectrometer equipped with the standard VG FAB ion source and an Ion Tech saddle-field atom gun. The atom gun controller was set at 1 A and 8 kV, with Xe for the bombarding atom beam, while the accelerator voltage was set to 8 kV.

Experiments that introduce the radical trap nitrosobenzene³⁸ were run under a nitrogen atmosphere using distilled and degassed acetonitrile. Solutions were prepared with 5 mM **3** and 100 mM nitrosobenzene, to which the base was added to 20 mM. Solutions were transferred to argon-flushed EPR tubes and frozen in liquid nitrogen. EPR spectra were obtained on a Bruker EMX spectrometer at X-band frequency (9.33 GHz). Typical microwave power was 20 mW, although further analysis of some spectra was accomplished using 125 mW, optimizing the 16-line signal relative to the organic radical signal at $g = 2.02$ due to greater saturation of the radical signal at that power. Control samples including each combination of two of the three above reactants were also run.

Single-crystal X-ray diffraction experiments were performed on a Siemens P4 automated diffractometer equipped with a LT-2 low-temperature apparatus at -95°C and graphite-monochromatized $\text{Mo K}\alpha$ radiation ($\lambda = 0.71073\text{ \AA}$). A crystal of approximate dimensions $0.34 \times 0.28 \times 0.24\text{ mm}$ was lightly coated with Paratone-N oil and flash frozen on a glass fiber. Reflection indexing and cell constants are based on a matrix of 40 well-centered reflections in the range $10.2^\circ \geq 2\theta \geq 24.9^\circ$. Additional details: scan method $\theta/2\theta$, scan rate variable 2–5 deg/min, background to scan ratio 0.5, 2θ scan range $5\text{--}52^\circ$ ($h, -1/14; k, -14/14; l, -17/18$), 8344 reflections measured, merged to

Table 1. Crystal Data for $[\text{Mn}^{\text{III}}(\text{salpn})(\text{Ph}_3\text{PO})](\text{CF}_3\text{SO}_3)\cdot\text{C}_6\text{H}_6\cdot 6\cdot\text{C}_6\text{H}_6$

formula	$\text{C}_{42}\text{H}_{37}\text{N}_2\text{O}_6\text{F}_3\text{MnPS}$
fw	840.71
cryst syst	triclinic
space group	$P1$
a (Å)	12.087(3)
b (Å)	12.119(3)
c (Å)	15.148(3)
α (deg)	68.970(10)
β (deg)	70.16(2)
γ (deg)	81.36(2)
vol (Å ³)	1947.2(7)
Z	2
ρ_{calcd} (mg/m ³)	1.434
temp (K)	178(2)
$F(000)$	868
abs coeff (mm ⁻¹)	0.499
limiting indices	$-1 \leq h \leq 14, -14 \leq k \leq 14,$ $-17 \leq l \leq 18$
Θ range (deg)	2.50–26.01
no. of reflns collected	8344
no. of indep reflns	7274 [$R(\text{int}) = 0.0477$]
no. of data/restraints/ params	7219/0/507
final R indices ($I > 2\sigma(I)$) ^a	$R1 = 0.0600, \text{w}R^2 = 0.1265$
R indices (all data) ^a	$R1 = 0.1453, \text{w}R^2 = 0.1503$

$$^a R1 = \sum ||F_o| - |F_c||/|F_o|; \text{w}R^2 = [\sum w(|F_o| - |F_c|)^2/\sum w|F_o|^2]^{1/2}.$$

7274 unique reflections, $R_{\text{int}} = 0.0477$, no correction for absorption applied. The structure was solved by direct methods, and 507 parameters were refined in a full matrix with the program SHELXTL PLUS.³⁹ The molecule lies on an inversion center with two benzene solvate molecules per dimer in the crystal lattice. All non-hydrogen atoms were allowed to refine anisotropically with hydrogen atoms placed in idealized positions. Neutral atom scattering factors and corrections for anomalous dispersion were taken from the *International Tables for Crystallography*.⁴⁰ Other details of the crystal structure, e.g., unit cell parameters, space group, and R values, are presented in Table 1.

X-ray Absorption Spectroscopy (XAS). Samples of **1**, **2**, and **3** were diluted in boron nitride (ca. 1:1 mass ratio) and ground to homogeneity using a mortar and pestle. Samples were then packed into a 1 mm thick Al cell with 30 μm Kapton windows and frozen immediately at 77 K. XAS spectra for **1** and **2** were collected at the National Synchrotron Light Source (NSLS) beam line X19-A, while data for **3** were collected at the Stanford Synchrotron Radiation Laboratory (SSRL) beam line 7-3. Both facilities were operated under dedicated conditions (2.5 GeV/200 mA and 3.0 GeV/100 mA, respectively). In both locations, XAS data were measured in absorption mode using N_2 -filled ionization chambers and a Si(220) double-crystal monochromator. Temperature was maintained at 10 K using an Oxford Instruments liquid He flow cryostat. Energy was calibrated using a KMnO_4 internal standard, with the KMnO_4 pre-edge transition defined as 6453.3 eV. Typical data sets consisted of an average of two spectra (at ca. 30 min/spectrum). Spectra were measured from 6300 to 7400 eV, with a k spacing of 0.05 \AA^{-1} .

Polynomial pre-edge subtraction, spline background removal, and EXAFS normalization followed standard procedures.⁴¹ The k^3 -weighted EXAFS was truncated at 1.0 and 11.5 \AA^{-1} . Data were Fourier transformed for visualization; see Figure 3. All of the best-fit parameters were determined from fitting unfiltered data. Theoretical models for the EXAFS amplitude and phase functions were calculated using the program FEFF 5.04.⁴² Theoretical EXAFS parameters were calculated for Mn–O, Mn–N, and Mn–Mn interactions. The scale factors and

(39) Sheldrick, G. M. SHELXTL-PLUS Structure Determination Programs, Siemens, Madison, WI, 1993.

(40) *International Tables for Crystallography*; Ibers, J. A.; Hamilton, W. C., Eds.; Knoch Press: Birmingham, 1974; Vol. 4.

(41) Riggs-Gelasco, P. J.; Mei, R.; Yocum, C. F.; Penner-Hahn, J. E. *J. Am. Chem. Soc.* **1996**, *118*, 2387–2399.

(42) Rehr, J. J.; Mustre de Leon, J.; Zabinsky, S. I.; Albers, R. C. *J. Am. Chem. Soc.* **1991**, *113*, 5135–5140.

(37) Izutsu, K. *Acid-Base Dissociation Constants in Dipolar Aprotic Solvents*; Blackwell Scientific Publications: Boston, 1990.

(38) Gronchi, G.; Tordo, P. *Res. Chem. Intermed.* **1993**, *19*, 733–753.

threshold energies were calibrated by using these parameters to fit crystallographically characterized Mn(IV) complexes, giving a scale factor of 0.9 for all shells, and threshold energies of 0.6, 0.6, and 14.6 eV for O, N, and Mn, respectively. Least-squares fits were used to determine Mn–ligand distances and coordination numbers as described previously.⁴¹ XANES spectra were normalized to match tabulated absorption coefficients both below and above the edge⁴³ using a single polynomial and scale factor.

Results

Synthesis of Oxo/Methoxo-Bridged Dimer and Comparison to Oxo/Hydroxo-Bridged Dimer. The complex $[\{\text{Mn}^{\text{IV}}(\text{salpn})\}_2(\mu\text{-O},\mu\text{-OCH}_3)](\text{CF}_3\text{SO}_3)$, **3**, is prepared by addition of excess methyl triflate to a dry methylene chloride solution of $[\text{Mn}^{\text{IV}}(\text{salpn})(\mu\text{-O})]_2$, **1**, and stirring at room temperature for 10–16 h. The yield is much lower than that of $[\{\text{Mn}^{\text{IV}}(\text{salpn})\}_2(\mu\text{-O},\mu\text{-OH})](\text{CF}_3\text{SO}_3)$, **2**, because the slow rate of methyl transfer requires a large excess of methyl triflate. The excess methyl triflate can react again with **3** to form $[\text{Mn}^{\text{IV}}(\text{salpn})(\mu\text{-OCH}_3)]_2^{2+}$ which is too unstable to isolate. However, the pure purple solid product may be obtained in useful yields upon removal of decomposition products and remaining starting materials, by making use of differential solubilities. The slow formation of **3** is in sharp contrast to the nearly instantaneous achievement of $\text{p}K_{\text{a}}$ -based equilibrium between **2** and various acids, allowing nearly 100% yield in formation of **2** using stronger acids. Substitution of the hydroxo bridge by the methoxo bridge provides significantly greater solubility in less polar solvents, such as methylene chloride, without loss of solubility in more polar solvents, such as acetonitrile and methanol.

Aside from the solubility difference, most of the physical and electronic properties of **3** and **2** are quite similar. The phenolate-to-Mn charge-transfer band (from the salpn ligand) in the UV/vis absorption spectrum is at 490 nm for **1**¹⁹ as compared to 514 nm for **3**, and 528 nm for **2** in acetonitrile; the latter two are shown as Figure 1A. Addition of 1 equiv of strong acid, protonating the second bridge, shifts this absorption to 632 or 638 nm, respectively, causing a color change to blue-green, Figure 1B, that rapidly bleaches to yellow-brown (370 nm) at room temperature in each complex. The slightly higher energy of the phenolate-to-manganese charge-transfer transitions in the methoxo-bridged complexes correlates with the somewhat poorer electron-withdrawing properties of the methyl group relative to the proton. This is consistent with the slightly lower cathodic (irreversible) reduction potential of **3**, at 0.252 V vs SCE, compared to 0.266 V for **2** in acetonitrile, Figure 2A. Although insolubility of $[\text{Mn}^{\text{IV}}(\text{salpn})(\mu\text{-OH})]_2(\text{CF}_3\text{SO}_3)_2$, **4**, at temperatures that prevent its decomposition precludes determination of its reduction potential, addition of 1 equiv of triflic acid to **3** in methylene chloride at $-35\text{ }^\circ\text{C}$ causes an increase of 0.4 V in its reduction potential, along with the color change to blue-green that indicates formation of $[\{\text{Mn}^{\text{IV}}(\text{salpn})\}_2(\mu\text{-OH},\mu\text{-OCH}_3)](\text{CF}_3\text{SO}_3)_2$, **5**, Figure 2B. This is 1.1 V higher than the cathodic wave in the reversible reduction of **1** in methylene chloride.²⁰ The $\text{p}K_{\text{a}}$ of **5** is within the error bars of the value we reported previously for **4**, 6.5 ± 1 in distilled acetonitrile at room temperature.²⁰

X-ray absorption spectroscopy also supports the similarity of these complexes. EXAFS analysis of **3** and **2** indicates that both complexes show a 0.1 Å increase in the Mn–Mn separation

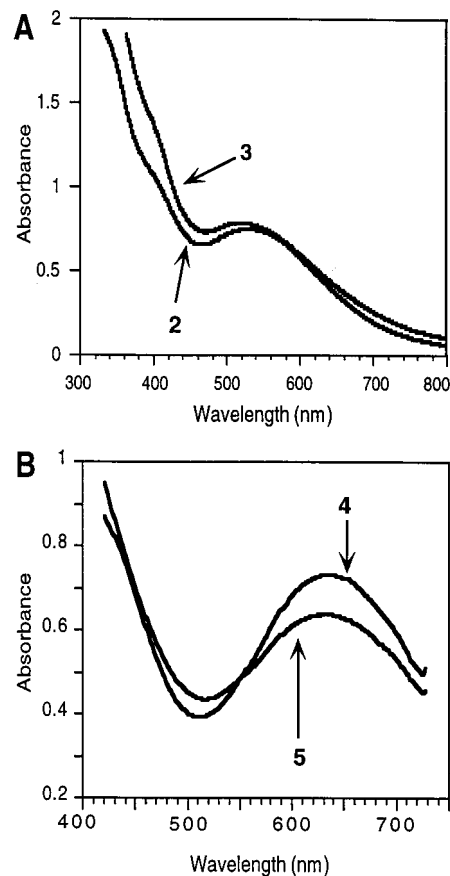


Figure 1. UV/vis absorption spectra of acetonitrile solutions of (A) $[\{\text{Mn}^{\text{IV}}(\text{salpn})\}_2(\mu\text{-O},\mu\text{-OH})](\text{CF}_3\text{SO}_3)$, **2**, and $[\{\text{Mn}^{\text{IV}}(\text{salpn})\}_2(\mu\text{-O},\mu\text{-OCH}_3)](\text{CF}_3\text{SO}_3)$, **3**, and (B) $[\text{Mn}^{\text{IV}}(\text{salpn})(\mu\text{-OH})]_2(\text{CF}_3\text{SO}_3)_2$, **4**, and $[\{\text{Mn}^{\text{IV}}(\text{salpn})\}_2(\mu\text{-OH},\mu\text{-OCH}_3)](\text{CF}_3\text{SO}_3)_2$, **5**.

(**3**, 2.82 Å; **2**, 2.85 Å) compared with the unperturbed $[\text{Mn}^{\text{IV}}(\mu\text{-O})]_2$ dimer, **1** (2.73 Å),¹⁷ Table 2 and Figure 3. The XANES spectra for **1**, **2**, and **3** are very similar, indicating that all three complexes are in the Mn^{IV}_2 oxidation level, Figure S2 in the Supporting Information. The 1s–3d transitions (inset to Figure S2) for all three complexes have similar areas, consistent with distorted octahedral geometries in each case. The 1s–3d transition for **2**, however, is significantly narrower, and correspondingly more intense, than those for **1** and **3**. This indicates that the details of 3d + 4p mixing vary depending on the identity of the bridging ligand. These differences do not, however, give significant changes in the electronic structure as determined by UV/vis spectroscopy.

Reactions with Hydrogen Peroxide. In methylene chloride, **1** is an effective catalyst of hydrogen peroxide disproportionation,^{15,22} while **2** reacts with H_2O_2 to produce 1/2 of catalytic **1**, as well as $[\text{Mn}^{\text{III}}(\text{salpn})]^+$ products which are unreactive with H_2O_2 in the absence of added base.¹⁶ The reaction of **3** and H_2O_2 in this solvent appears to be nearly identical to that of **2**. These reactions are quantified by monitoring the loss of the 514 nm absorbance of **3** and the increase of the shoulder at 490 nm, which is characteristic for **1**. In acetonitrile, **1** does not react with H_2O_2 , so excess H_2O_2 is not catalytically consumed by reaction products of **2** or **3**. In this solvent, **3** reacts with excess H_2O_2 to form half an equivalent of **1** and an equivalent of a $[\text{Mn}^{\text{III}}(\text{salpn})]^+$ complex (Scheme 1A,B), with no further reaction until additional base is added (Scheme 1C). Addition of 1 equiv of tributylamine to this product mixture results in the oxidation of the Mn^{III} complex to **1** by some of the remaining H_2O_2 (Scheme 1C), with a total yield of 100% of **1**. This demonstrates

(43) McMaster, W. H.; Del Grande, N. K.; Mallett, J. H.; Hubbel, J. H. *Compilation of X-ray Cross Sections*; National Technical Information Services: Springfield, 1969; Vol. UCRL-50174.

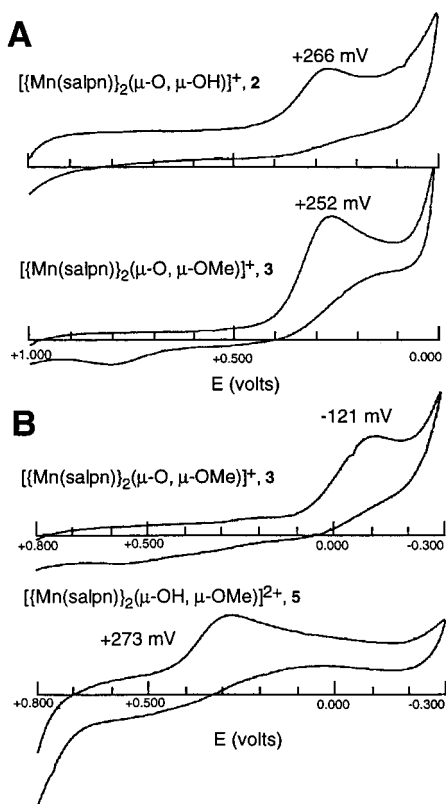


Figure 2. Cyclic voltammograms comparing (A) $[\{\text{Mn}^{\text{IV}}(\text{salpn})\}_2(\mu\text{-O}, \mu\text{-OCH}_3)](\text{CF}_3\text{SO}_3)$, **2**, and $[\{\text{Mn}^{\text{IV}}(\text{salpn})\}_2(\mu\text{-O}, \mu\text{-OH})](\text{CF}_3\text{SO}_3)$, **3**, in acetonitrile at room temperature vs SCE and (B) **3** and **5** in methylene chloride at $-35\text{ }^\circ\text{C}$ vs Ag wire.

Table 2. EXAFS Fitting Results for **1–3**

complex	Mn–O/N			Mn–Mn		
	R (Å)	CN ^a	σ^2 ^b	R (Å)	CN ^a	σ^2 ^b
1 ^c	1.88	4.0	4.9	2.73	1.0	2.5
2 ^c	1.89	3.0	4.2	2.82	1.0	3.8
3	1.88	3.5	4.9	2.85	1.0	3.9

^a Coordination numbers are given as the best fit integer value.

^b Debye–Waller factors are given in units of $\text{Å}^2 \times 10^3$. ^c Reported previously in ref 19.

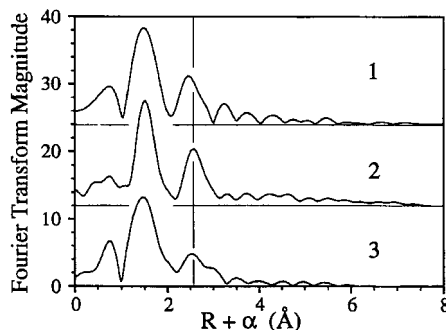


Figure 3. Fourier transforms of the EXAFS data for $[\text{Mn}^{\text{IV}}(\text{salpn})(\mu\text{-O})]_2$, **1**, $[\{\text{Mn}^{\text{IV}}(\text{salpn})\}_2(\mu\text{-O}, \mu\text{-OH})](\text{CF}_3\text{SO}_3)$, **2**, and $[\{\text{Mn}^{\text{IV}}(\text{salpn})\}_2(\mu\text{-O}, \mu\text{-OCH}_3)](\text{CF}_3\text{SO}_3)$, **3**. The vertical line drawn at $R + \alpha = 2.4$ (i.e., $R \approx 2.8\text{ Å}$) indicates the approximate vertical position of the Mn–Mn peak. Spectra offset vertically by 10 and 20 for clarity.

the importance of the base equivalents on the oxo bridges in the hydrogen peroxide disproportionation catalysis. Addition of the weak acid pyridinium ($\text{p}K_a = 12.3$ in acetonitrile, compared to ~ 6.5 for **4** or **5**), which is far too weak to protonate the second bridge on **2** or **3**, completely inhibits the reaction of H_2O_2 with either **2** or **3**.

Scheme 1

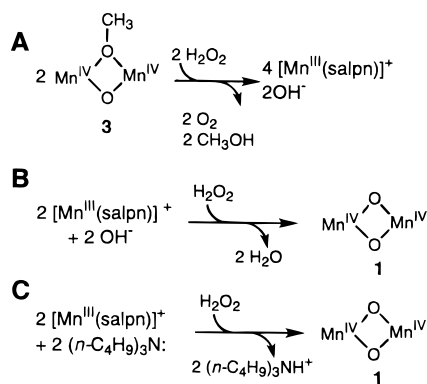


Table 3. Bases Used in Reactions with **3** and Their $\text{p}K_a$ Values in CH_3CN , Oxidation Potentials, $\text{N}(\text{O})\text{-H}$ BDEs, and Relative Rate Constants

base	$\text{p}K_a$, conjugate acid ^a	potential (V vs. SCE) ^b	BDE of BH^+ (kcal/mol)	relative rate const.
aniline	10.6	0.92	94	0.038
<i>N,N</i> -dimethylaniline		0.72		0.032
pyridine	12.4	>2		<0.002
2,4-lutidine	14.1	>2		<0.002
tributylamine	18.1	0.76	100	0.78
triethylamine	18.5	0.81	102	1 ^c
pyrrolidine	19.6	1.03	109	0.24
quinuclidine	19.5	1.07	109	8.6
proton sponge	~ 20	0.33	93	140
acetate	22.3	1.18	116	98
1,1,3,3-tetramethylguanidine	23.3	1.24	119	38
triphenylphosphine		1.13		
3	6.5	0.25	76	

^a References 20 and 37. ^b The Experimental Section details collection of this data. ^c Rate constant of Et_3N arbitrarily defined as 1.

Reactions with Amines and Triphenylphosphine. The reaction of **2** with bases whose conjugate acids have higher $\text{p}K_a$ values in acetonitrile, such as acetate and many amines, consists simply of rapid proton transfer, resulting in **1** as the sole manganese product. The corresponding reactions of **3** appear to give the same manganese product, though more slowly. However, $^{18}\text{O}_2$ labeling of the bridging oxygen atoms indicates that, while no bridge exchange occurs in the simple proton-transfer reaction of **2**, the reaction of **3** results in exchange of the bridging oxygen atoms with oxygen atoms from trace water in the solvent. In the absence of the base, no bridge exchange is observed, nor is bridge exchange observed for **1** in the presence of even very high concentrations of tributylamine. Additionally, no evidence has been found in experiments monitored by NMR, gas chromatography, or mass spectrometry for methyl transfer to the reactant base. Methyl transfer is not even observed in the reaction of **3** with benzenethiolate from $[\text{Zn}(\text{PhS})_4]^{2-}$, which has been shown to have a propensity for methyl cation abstraction.⁴⁴

In stopped-flow experiments monitored by a rapid-scanning monochromator allowing observation of the spectral range from 400 to 700 nm as often as once per millisecond, no spectroscopically resolvable intermediate is observed in the reaction of **3** with a series of amines and acetate. Reactions of the bases listed in Table 3 which are as fast or faster than the reaction of triethylamine show an isosbestic conversion from **3** to **1**, while the slower reactions result in a loss of up to 30% of the charge-

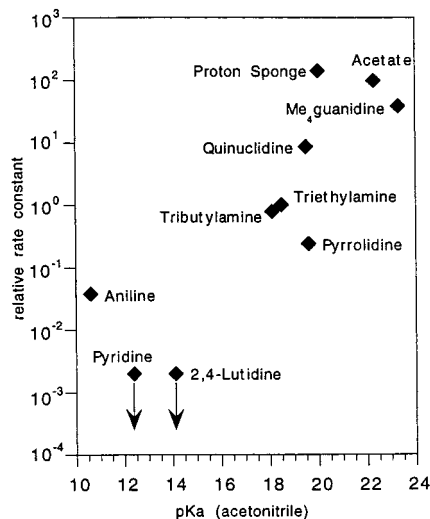


Figure 4. Relative rates of reaction of $[\{\text{Mn}^{\text{IV}}(\text{salpn})\}_2(\mu\text{-O},\mu\text{-OCH}_3)]\text{-}(\text{CF}_3\text{SO}_3)$, **3**, with various bases vs the $\text{p}K_{\text{a}}$ of the conjugate acid.

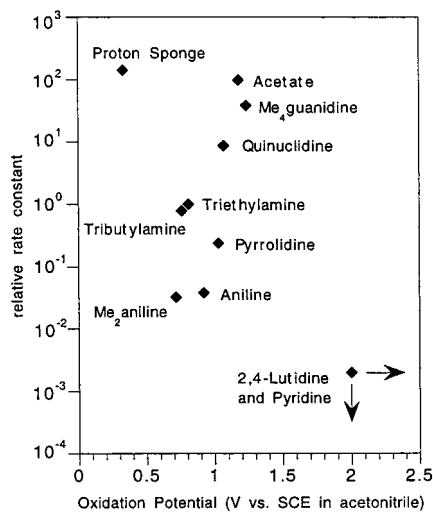


Figure 5. Relative rates of reaction of $[\{\text{Mn}^{\text{IV}}(\text{salpn})\}_2(\mu\text{-O},\mu\text{-OCH}_3)]\text{-}(\text{CF}_3\text{SO}_3)$, **3**, with various bases vs the cathodic potential of the base.

transfer intensity as the same conversion occurs. In addition, the spectra of the solutions resulting from the reactions with aniline and dimethylaniline show significant broadening of the high-wavelength side of the 490 nm shoulder, suggesting a contribution from either **2** or **3**. The rates of these reactions increase with increasing concentration of trace water (up to at least 0.05%, or 28 mM) in the CH_3CN solvent. This effect is not entirely due to a change in the properties of the solvent with added water, as a deuterium isotope effect of $k_{\text{H}}/k_{\text{D}} = 2.2 \pm 0.4$ is observed for the reaction of 0.05 mM **3** and 2.5 mM triethylamine in distilled CH_3CN with 0.05% H_2O or D_2O .

In comparing the rate of reaction with the amines listed in Table 3, a general trend of increasing rate with increasing $\text{p}K_{\text{a}}$ is observed. There is significant scatter in a plot of this trend, however, with the rates for pyridine and lutidine being anomalously slow, Figure 4. The rate appears to correlate better with the cathodic potential for the oxidation of the base, except for those bases at the extremes of the potential range, Figure 5. This correlation suggests a redox role for the base. To determine if an amine radical is formed in the reactions with **3**, the reactions were run anaerobically in the presence of the radical trap, nitrosobenzene. EPR spectra of the reaction products revealed that the slower reactions resulted in a strong radical signal, Figure 6A, while the faster reactions resulted in a 16-

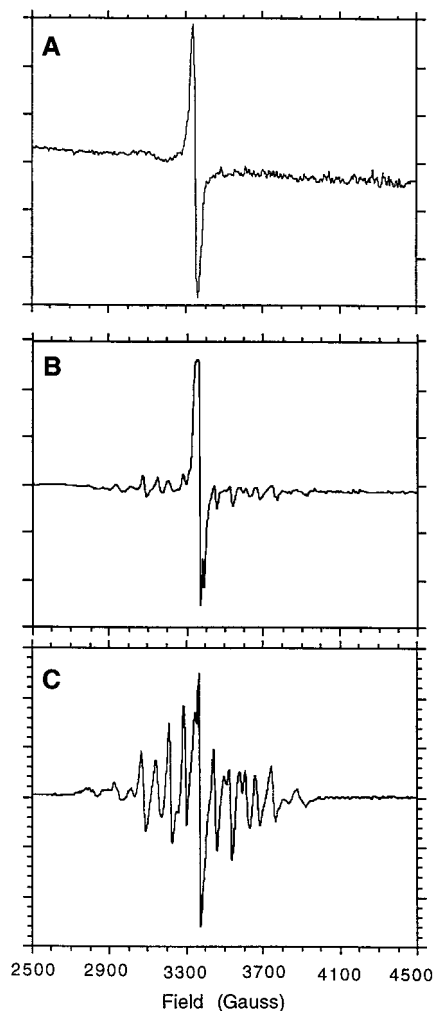


Figure 6. EPR spectra of acetonitrile solutions of $[\{\text{Mn}^{\text{IV}}(\text{salpn})\}_2(\mu\text{-O},\mu\text{-OCH}_3)]\text{-}(\text{CF}_3\text{SO}_3)$, **3**, and nitrosobenzene after addition of (A) *N,N*-dimethylaniline, (B) tributylamine, or (C) 1,1,3,3-tetramethylguanidine.

line signal with a hyperfine splitting of about 80 G, Figure 6C. The exception is the fast reaction of “proton sponge”, which produces no EPR signal. Reactions of intermediate rate gave spectra with a mixture of these two signals, Figure 6B. The 16-line signal is characteristic of strongly coupled $\text{Mn}^{\text{III}}\text{Mn}^{\text{IV}}$ dimers, and does not appear in the reaction mixture in the absence of a radical trap. The UV/vis spectra of the anaerobic reaction product of **3** with most of the bases and the radical trap show the presence of the 490 nm absorption characteristic of either the $\text{Mn}_2^{\text{III,IV}}$ or $\text{Mn}_2^{\text{IV,IV}}$ bis(oxo)-bridged dimer (i.e., **1** or its one-electron-reduced derivative), but lacks sufficient intensity to indicate complete formation of the fully oxidized **1**. Again, the exception is a proton sponge, which results in a spectrum more consistent with Mn^{III} products. In contrast, the anaerobic reaction of each base without the radical trap forms **1** in 70–100% yield, depending on the reactant base as described above for the aerobic reactions.

The reaction of **3** with triphenylphosphine results in the nearly stoichiometric production of triphenylphosphine oxide. The Ph_3PO product was identified by FAB-MS, and quantitated by gas chromatography. The yield was 0.86 ± 0.22 molecules of Ph_3PO per Mn dimer in air and 0.8 ± 0.2 per dimer under anaerobic conditions. Isotopic labels from the oxygen bridges of the Mn complex¹⁵ are not incorporated into the Ph_3PO product, while labels from small amounts of H_2^{18}O added to the acetonitrile solvent are incorporated into the product. Neither **1** nor **2**

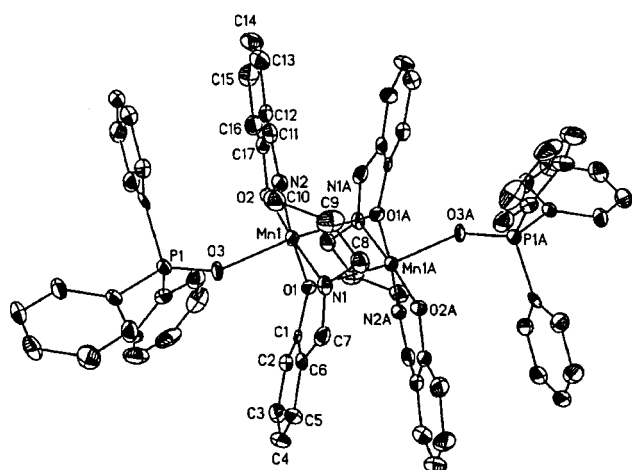
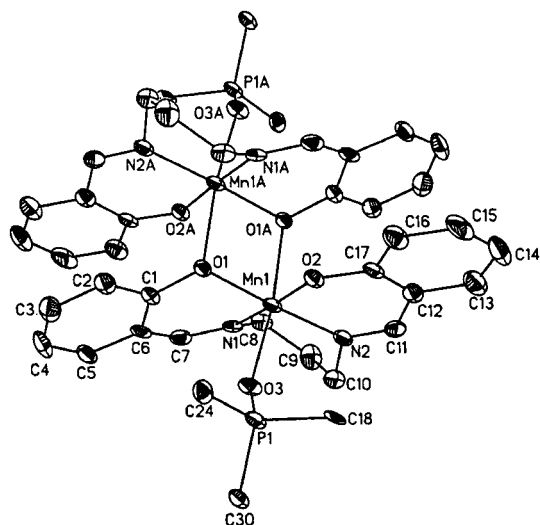


Figure 7. Crystal structure of $[\text{Mn}^{\text{III}}(\text{salpn})(\text{Ph}_3\text{PO})](\text{CF}_3\text{SO}_3)$, **6**. The top ORTEP view clearly shows the structure of the $[\text{Mn}^{\text{III}}(\text{salpn})]^+$ units and the bridging phenolate interactions of the solid-state dimerized complex $[\text{Mn}^{\text{III}}(\text{salpn})(\text{Ph}_3\text{PO})]^+$, which forms the $[\text{Mn}^{\text{III}}(\text{salpn})(\text{Ph}_3\text{PO})]_2^{2+}$ dimer presented here. The full phenyl rings of the Ph_3PO moieties have been omitted for clarity. The bottom ORTEP provides a better view of the $\text{Mn}^{\text{III}}\text{-Ph}_3\text{PO}$ interactions. Thermal ellipsoids are shown at 30% probability.

oxidizes triphenylphosphine to its oxide. While this reaction appears to produce some **1** when run in air, it is not produced in yields which approach those of the amine reactions. Thus, while the reaction of **3** with Ph_3P has some features in common with the amine reactions, both the Mn and substrate products are different.

The FAB^+ mass spectrometry experiments used to analyze the Ph_3P reactions show a peak at m/z 335, $[\text{Mn}^{\text{III}}(\text{salpn})]^+$, in addition to a peak consistent with Ph_3PO at m/z 279, and a peak at m/z 613. This higher mass peak corresponds to the $[\text{Mn}^{\text{III}}(\text{salpn})(\text{Ph}_3\text{PO})]^+$ adduct. This complex can be synthesized independently by addition of excess triphenylphosphine oxide to a solution of $[\text{Mn}^{\text{III}}(\text{salpn})(\text{H}_2\text{O})_2](\text{CF}_3\text{SO}_3)$. The IR spectrum of the Ph_3PO adduct has most of the same features of both $[\text{Mn}^{\text{III}}(\text{salpn})(\text{H}_2\text{O})_2](\text{CF}_3\text{SO}_3)$ and Ph_3PO , except that the strong $\text{P}=\text{O}$ stretch has disappeared or shifted significantly. This is consistent with loss of the double bond character upon coordination to manganese. The crystal structure of $[\text{Mn}^{\text{III}}(\text{salpn})(\text{Ph}_3\text{PO})](\text{CF}_3\text{SO}_3)$, **6**, has been solved and is shown in Figure 7. Selected bond distances and angles are listed in Table 4. The structure shows dimerization in the solid state, with each Mn

Table 4. Selected Bond Lengths (Å) and Angles (deg) for **6**

Bond Lengths			
Mn1—O1	1.914(3)	Mn1—O3	2.131(3)
Mn1—O1A	2.339(3)	Mn1—N1	2.007(4)
Mn1—O2	1.869(3)	Mn1—N2	1.973(4)
Angles			
O1—Mn1—N1	88.0(2)	O2—Mn2—N2	90.6(2)
O1—Mn1—N2	175.2(2)	O3—Mn1—O1A	172.34(12)
O1—Mn1—O1A	80.48(14)	N1—Mn1—O1A	84.58(14)
O1—Mn1—O3	94.41(14)	N1—Mn1—O3	89.57(14)
O2—Mn1—O1	91.3(2)	N2—Mn1—N1	89.8(2)
O2—Mn1—O1A	91.34(13)	N2—Mn1—O1A	95.14(14)
O2—Mn1—O3	94.49(13)	N2—Mn1—O3	89.8(2)
O2—Mn1—N1	175.9(2)	Mn1—O1—Mn1A	99.52(14)

ion having four equatorial donors from one salpn^{2-} , an axial oxygen donor from Ph_3PO , and axial ligation to a phenolate oxygen of the neighboring salpn^{2-} ligand. This structure of the Ph_3PO portion of the molecule is similar to the structure of $[\text{Mn}^{\text{III}}(\text{tetra-bromocatecholato})_2(\text{Ph}_3\text{PO})]$ reported by Pierpont, Dolcetti, and co-workers,⁴⁵ while dimerization of the salpn^{2-} ligand is reminiscent of $[\text{Mn}^{\text{III}}(\text{salen})\text{Cl}]_2$.⁴⁶

Discussion

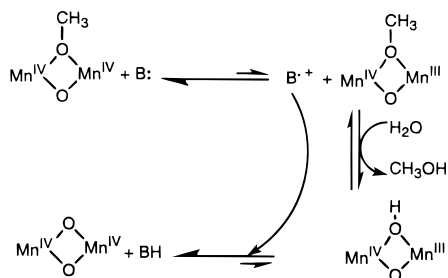
The oxo/methoxo-bridged dimer $[\{\text{Mn}^{\text{IV}}(\text{salpn})\}_2(\mu\text{-O},\mu\text{-OCH}_3)](\text{CF}_3\text{SO}_3)$, **3**, is formed by methylation of the bis(oxo)-bridged dimer $[\text{Mn}^{\text{IV}}(\text{salpn})(\mu\text{-O})_2]$, **1**, in a manner similar to (though more slowly than) that of the oxo/hydroxo-bridged dimer $[\{\text{Mn}^{\text{IV}}(\text{salpn})\}_2(\mu\text{-O},\mu\text{-OH})](\text{CF}_3\text{SO}_3)$, **2**. The similarity between spectroscopic features and electrochemical potentials of **2** and **3**, and the pK_a values of their protonation products $[\text{Mn}^{\text{IV}}(\text{salpn})(\mu\text{-OH})_2](\text{CF}_3\text{SO}_3)_2$, **4**, and $[\{\text{Mn}^{\text{IV}}(\text{salpn})\}_2(\mu\text{-OH},\mu\text{-OCH}_3)](\text{CF}_3\text{SO}_3)_2$, **5**, indicate that **3** is analogous to **2** in both geometric and electronic structure. Isotopic labeling of the oxo bridges has shown that the bridges are the *thermodynamic* site of protonation for the rapidly exchanging protons.¹⁹ The oxo-bridge-methylated structure of **3** indicates that this is also the *kinetic* site of alkylation (and, by analogy, of protonation), as the methyl groups are not labile, in contrast to the protons. The methylated analogue also facilitates study of the effects of oxo bridge protonation in the absence of the complications of proton lability. Indeed, **2** and **3** share similar reactivity with both strong acids and hydrogen peroxide. The difference in their reactivity with hydrogen peroxide compared to **1** is due to their deficiency in base equivalents available from the oxo bridges. One of these base equivalents is occupied by the proton or methyl cation of **2** or **3**, respectively, preventing these dimers from being capable of the hydrogen peroxide disproportionation catalysis of which **1** is so efficient.

In contrast to the similarities discussed above, the reactions of **2** and **3** with various amines and acetate, as well as triphenylphosphine, differ substantially. The reaction of **2** with the amine and acetate bases is a simple and rapid proton transfer to reach the pK_a -determined equilibrium. The reaction of these bases with **3** results in the same thermodynamically favored Mn product **1**; however, the mechanism is much different. In this case, the reaction is not only slower but also more complicated, as indicated by the exchange of the bridging oxygen atoms with water in the solvent. Thus, the lability of the proton in **2** results in the very fast proton transfer which circumvents the slower reaction seen for **3**. The reaction of **3**, then, is the result of the activation of the bis(oxo)-bridged dimer

(45) Larsen, S. K.; Pierpont, C. G.; DeMunno, G.; Dolcetti, G. *Inorg. Chem.* **1986**, *25*, 4828–4831.

(46) Pecoraro, V. L.; Butler, W. M. *Acta Crystallogr.* **1986**, *C42*, 1151–1154.

Scheme 2



by addition of a positive charge to an oxo bridge, while this "inherent" reactivity is lost to the rapid proton lability of **2**.

The lack of any evidence for methylation of the bases used in the reactions with **3**, even of PhS^- , as well as exchange of the bridging oxygen atoms with trace water in the solvent, indicates that the base-mediated conversion of **3** to **1** is not simply the methyl cation analogue of the proton-transfer reaction of **2**. The bridge exchange provides the first suggestion of the involvement of a redox step in this reaction, as the $\text{Mn}_2^{\text{IV,IV}}$ (d^3, d^3) dimers do not undergo bridge exchange, while reduction to $\text{Mn}_2^{\text{III,IV}}$ (d^4, d^3) causes lability of the bridging ligands. The presence of a redox step in the reaction mechanism is confirmed by the radical trap experiments monitored by EPR spectroscopy. In the presence of nitrosobenzene, which is oxidized by one electron to form a stable radical, the reaction results in a reduced Mn species and a nitrosobenzene-trapped radical. This is consistent with a mechanism in which a small portion of **3** is reduced by the base. Reoxidation of the reduced form of **3** then occurs, occasionally after exchange of a methoxy bridge for a hydroxo bridge from water in solution. The reoxidized Mn dimer will be deprotonated by the base if the bridge exchange has occurred, forming **1**. This reoxidation and deprotonation may occur in two separate steps or as a single-step hydrogen atom transfer. In the presence of nitrosobenzene, the oxidized amine radical is trapped, producing the stable radical signal in the EPR spectrum. This signal is more pronounced for the lower potential bases, as the radicals of the higher potential bases are unlikely to be sufficiently long-lived to be trapped by nitrosobenzene in sufficiently high yield to be easily observed. This trapping of the amine cation radical removes the oxidant that is necessary for reoxidation of the Mn, leaving reduced Mn species including the $\text{Mn}_2^{\text{III,IV}}$ dimer observed in the EPR spectrum, Figure 6C. This signal is most pronounced for the high $\text{p}K_a$ bases, as the very basic $\text{Mn}_2^{\text{III,IV}}$ dimer disproportionates in the presence of acidic protons. The lowest $\text{p}K_a$ bases, aniline and dimethylaniline, show no 16-line EPR signal, Figure 6A. In fact, the product of these bases includes some **2**, as they are not sufficiently basic to completely deprotonate the oxo bridge, even in the large excess of base with which these reactions are run.

On the basis of the above observations, at least three general steps are necessary in the reaction of **3** with amine to form **1**, with no apparent alteration to the amine in the product mixture except perhaps protonation. The first step is reduction of **3**, with concurrent oxidation of the amine. Next, either charge recombination occurs with return to reactants or a labilized bridge exchanges with water in the solvent, converting **3** to the reduced derivative of **2**. This intermediate is then reoxidized by the amine cation radical and deprotonated, either in a single step with oxidation as a hydrogen atom transfer or in consecutive steps. This general mechanism is shown in Scheme 2. The kinetically observed deuterium isotope effect in this reaction may result either from an equilibrium isotope effect in step 2, which manifests itself as a decrease in the rate at which **3** is converted

to **1** due to a decrease in conversion of **3** to **2** in the presence of D_2O , or from an authentic kinetic isotope effect if the detailed mechanism of step 3 includes a hydrogen atom transfer.

Superficially, one would expect the rate of the reaction in Scheme 2 to be faster for bases which are more easily oxidized by **3**. However, the relative reaction rates for the bases in Table 3 are the inverse of that expectation, with the higher potential bases (excluding the two bases which are at least 2 V higher in potential than **3**) showing faster reaction rates. As observed for other properties of this reaction, proton sponge deviates from this trend, likely proceeding by a different mechanism allowed by the similarity of its potential to that of **3**. The potential of the proton sponge exceeds that of **3** by less than 0.1 V, while the potentials of other bases in Table 3 exceed the potential of **3** by 0.5 V or more. The relative rates of the reactions of these other bases must result from the establishment of steady-state equilibria in steps 1 and 2 of Scheme 2, with the differences in reaction rates determined by the rate at which step 3 is driven to completion. If step 3 consists of separate Mn oxidation and oxo bridge deprotonation steps, one might expect the faster rate of step 3 for the higher potential bases to be compensated by the much lower steady-state equilibrium constant for step 1, making the 5 orders of magnitude difference in the relative rates for different bases somewhat surprising. On the other hand, the higher potentials also correlate with higher $\text{p}K_a$ values, except for the outliers at the extremes. Thus, for a hydrogen atom transfer step the difference in rate will be determined by the thermodynamic driving force due to the N(or O)–H bond dissociation energy (BDE) of protonated base (listed in Table 3) minus the O–H bond dissociation energy of the reduced derivative of **2**, determined previously to be 76 kcal/mol.²⁰ In this case, the combined trend in potential and $\text{p}K_a$ which contributes to the BDE is unlikely to be well compensated by the difference in the equilibrium of step 1, and the 5 orders of magnitude difference in rate may be expected.

The reaction of triphenylphosphine with **3** results in oxygenation of the phosphine to its oxide, and reduction of the manganese. Isotopic labeling studies show that this reaction is not the typical oxygen atom transfer often associated with Ph_3P , but is likely related to the amine reactions. The oxidation potential for triphenylphosphine is in the same range as those of acetate and the amine bases which react with **3** in the manner described above. However, it is not nearly as strong a base, so the driving force associated with step 3 in Scheme 2 is not as great. In addition, the greater affinity of the phosphine for oxygen compared to the amines allows the oxidized phosphine to be intercepted by a water molecule in the solvent, resulting in formation of the oxide rather than a back-reaction with the reduced Mn species. The phosphine is also not sufficiently basic to promote the air oxidation of the reduced Mn species. Thus, the initial step in the oxidation of Ph_3P by **3** is likely the same as for most of the amines, while the following steps differ due to its lower basicity and greater oxophilicity. If **2** is used in this reaction rather than **3**, no Ph_3PO is formed. This is likely due to hydrogen bonding with the Ph_3P substrate. Ph_3P is capable of deprotonating **4** by one proton at -40°C in acetonitrile, and is thus likely to be able to hydrogen bond to **2** rather strongly. This would simultaneously make **2** more **1**-like, modulating its reactivity as an oxidant, and make the substrate less susceptible to oxidation by occupying some of the electron density of its available lone electron pair. Again, we see the "inherent" activation of the complex by oxo bridge protonation

modulated by the hydrogen bonding or lability properties of the proton–oxygen bond in **2** relative to the carbon–oxygen bond of **3**.

These studies demonstrate that methylation of an oxo bridge in this transition metal dimer is a good analogue for protonation, in terms of electronic structure and spectroscopic and electrochemical features, as well as reactivity with certain substrates. In other reactions, however, significant differences in behavior are observed. These differences may be attributed to the ability of the proton to hydrogen bond or dissociate. The methyl group lacks these properties. This observation suggests that care should be exercised when the reactivity of protonated oxo-bridged complexes that may be acidic is interpreted. Under appropriate conditions, the true reactivity of a compound may be masked by a rapid proton transfer to a more basic substrate, which deactivates the system.

Comparison of the reaction mechanisms of the protonated and methylated complexes provides insight into the effects of hydrogen bonding and proton lability upon the inherent activation of the complex due to addition of a positive charge to the oxo bridge. The reactions cited here show complete deactivation of a redox mechanism due to lability or hydrogen-bonding by the proton. In a metalloprotein active site, the hydrogen bonding ability of the proton may be used to fine-tune the reactivity of the oxo-bridged active site. The propensity of the active site environment for hydrogen bonding, the direction of substrate approach, and dielectric effects on proton lability may all contribute to modulation of proton-activation of enzymatic catalysis. The redox mediation by amines in the reactions discussed here also suggests a novel role for amines in enzyme active sites. Redox activity of endogenous tyrosine, tryptophan, or other amino acid residues is known to be required for the

functioning of a number of enzymes.^{47–51} The reactions discussed above demonstrate the feasibility of amino groups as transient redox mediators in some metalloenzyme reactions as well.

Acknowledgment. The authors wish to acknowledge the helpful discussions and suggestions from Dr. M. Tyler Caudle in our laboratory. Funding was provided by the National Institutes of Health to V.L.P. (Grant GM39406) and to J.E.P.H. (Grant GM45205). XAS data were measured in part at SSRL and NSLS, which are operated by the Department of Energy, Office of Basic Energy Sciences, with additional support to the SSRL Biotechnology Program from the National Institutes of Health, National Center for Research Resources Biomedical Technology Program, and by the Department of Energy, Office of Biological and Environmental Research.

Supporting Information Available: Tables listing crystallographic data, including bond distances and angles, anisotropic parameters, and atomic coordinates, and Figures S1, k^3 -weighted EXAFS data, and S2, normalized XANES spectra, for **1**, **2**, and **3**. This material is available free of charge via the Internet at <http://pubs.acs.org>.

IC990346E

-
- (47) Stubbe, J. A. *Annu. Rev. Biochem.* **1989**, *58*, 257–285.
(48) Metalloenzymes Involving Amino Acid-Residue and Related Radicals; Sigel, H., Sigel, A., Eds.; Metal Ions in Biological Systems; Marcel Dekker: New York, 1994; Vol. 30.
(49) Fontecave, M.; Pierre, J. C. *Bull. Soc. Chim. Fr.* **1996**, *133*, 653–660.
(50) Babcock, G. T.; Espe, M.; Hoganson, C.; Lydakis-Simantiris, N.; McCracken, J.; Shi, W.; Styring, S.; Tommos, C.; Warncke, K. *Acta Chem. Scand.* **1997**, *51*, 533–540.
(51) Stubbe, J.; van der Donk, W. A. *Chem. Rev.* **1998**, *98*, 705–762.